Acta Oceanol. Sin., 2022, Vol. 41, No. 7, P. 97–112
https://doi.org/10.1007/s13131-021-1974-0
http://www.aosocean.com
E-mail: ocean2@hyxb.org.cn

Long-term trend analysis of wave characteristics in the Bohai Sea based on interpolated ERA5 wave reanalysis from 1950 to 2020

Jichao Wang[1]*, Peidong Sun[1], Zhihong Liao[2], Fan Bi[3], Guiyan Liu[4]

[1] College of Science, China University of Petroleum, Qingdao 266580, China

[2] National Meteorological Information Center, Beijing 100081, China

[3] North China Sea Marine Forecasting Center of State Oceanic Administration, Qingdao 266061, China

[4] Shandong Provincial Key Laboratory of Marine Ecological Environment and Disaster Prevention and Mitigation, Qingdao 266061, China

Received 8 April 2021; accepted 3 September 2021

Abstract

Reasonably understanding of the long-term wave characteristics is very crucial for the ocean engineering. A feedforward neural network is operated for interpolating ERA5 wave reanalysis in this study, which embodies a detailed record from 1950 onwards. The spatiotemporal variability of wave parameters in the Bohai Sea, especially the significant wave height (SWH), is presented in terms of combined wave, wind wave and swell by employing the 71 years (1950–2020) of interpolated ERA5 reanalysis. Annual mean SWH decreases at –0.12 cm/a estimated by Theil-Sen estimator and 95th percentile SWH reflecting serve sea states decreases at –0.20 cm/a. Inter-seasonal analysis shows SWH of wind wave has steeper decreasing trend with higher slopes than that of swell, especially in summer and winter, showing the major decrease may attribute to the weakening of monsoon. The inner Bohai Sea reveals a general decreasing trend while the intersection connecting with the Yellow Sea has the lower significance derived by Mann-Kendall test. Meanwhile, 95th percentile SWH decreases at a higher rate while with a lower significance in comparison with the mean state. The frequencies of mean wave directions in sub-sector are statistically calculated to find the seasonal prevailing directions. Generally, the dominant directions in summer and winter are south and north. A similar variation concerning to SWH, the trend of the mean wave period is provided, which also shows a decrease for decades.

Key words: wave characteristic, wind wave, swell, long-term trend, Bohai Sea

Citation: Wang Jichao, Sun Peidong, Liao Zhihong, Bi Fan, Liu Guiyan. 2022. Long-term trend analysis of wave characteristics in the Bohai Sea based on interpolated ERA5 wave reanalysis from 1950 to 2020. Acta Oceanologica Sinica, 41(7): 97–112, doi: 10.1007/s13131-021-1974-0

1 Introduction

Wave characteristics are of paramount importance to coastal engineering projects, ship routings, oil platforms, designing and constructing of ports, and other human activities (Lv et al., 2014). The random, multi-scale wave characteristics are commonly described by the wave parameters consisting mainly of significant wave height (SWH), mean wave period (MWP), mean wave direction (MWD), etc. Wave climate refers to the average statistical characteristics of ocean wave parameters over several decades and their changes with time under the background of climate change (Bacon and Carter, 1991; Haxel and Holman, 2004). The impact of the long-term trends in the wave climate is exampled to be not negligible on the ocean engineering projects (Vanem and Bitner-Gregersen, 2012).

As the largest petroleum-bearing area in China, the Bohai Sea, which hosts intensive human activities and its rim region has become the economic heart of northern China, performs an important role in the strategy of economic development in China. Therefore, analyzing the long-term wave characteristics in the Bohai Sea will make a great contribution to guiding the projects in this area.

A number of studies on the wave conditions in the Bohai Sea have been conducted to determine the wave climate variation. Sun (1991) analyzed the wave characteristics in the west shore area of the Bohai Bay by using the measured data. Based on statistical calculation and post reporting methods, Teng and Wu (1994) studied the basic characteristics of annual extreme and design waves in the southern Bohai Sea. Yin et al. (2001) used a combined numerical model to study the influence of waves on tide-surges in the Bohai Sea. The joint probability distribution of wind speed and SWH in the Bohai Bay from 1989 to 2008 was investigated in Yang and Zhang (2013). Lv et al. (2014) applied the Simulating Waves Nearshore (SWAN) model to investigate the wave characteristics in the Bohai Sea for the period from 1993 to 2012. The wave climate of the Bohai Sea from 1990 to 2011 was investigated in Liang et al. (2016), where the spatial distributions of SWH were provided. Ren et al. (2017) analyzed the variation characteristics of the Bohai Sea wave climate by the usage of SWAN. After evaluating the performance of seven wind resources, Wu et al. (2020) simulated SWH in their considered re-

Foundation item: The National Natural Science Foundation of China under contract No. 42176011; the Shandong Provincial Natural Science Foundation under contract No. ZR2020MD060; the Fundamental Research Funds for the Central Universities under contract No. 19CX05003A-5.

*Corresponding author, E-mail: wangjc@upc.edu.cn

gion (the Bohai Sea, Yellow Sea, and East China Sea) for the year 2016.

Despite these researchers above have made enormous achievements, they were mainly devoted to the spatial distribution characteristics and focused only on the mixed wave field. There are two main classes of waves at the ocean surface: local wind wave and remotely generated swell waves, where mostly the latter are that dominate the global ocean (Semedo et al., 2011). The more detailed qualitative look on the impact of climate change on regional wind sea and swell climates needs to be pursuit (Semedo et al., 2015). Hence, it is still necessary to analyze the spatiotemporal variability of wind wave and swells in the Bohai Sea. Also, the length of time series in the previous study is generally 20 years, which is insufficient for the long-term trend analysis.

The main aim of this study is to present the long-term (71 years, 1950–2020) climatology of combined wave, wind wave and swell in the entire Bohai Sea on the basis of the interpolated high-resolution ERA5 reanalysis at 0.125°×0.125°, which is achieved by a machine learning algorithm, feedforward neural network (FFNN).

The arrangement of this paper is as follows. The study area and ERA5 reanalysis are presented in the following section. Section 3 describes the methodologies of trend analysis and spatial interpolation by FFNN. In Section 4, the main results of the long-term variability and the spatiotemporal distribution of wave characteristics in the area of interest are investigated. Finally, the conclusions derived are given in Section 5.

2 Study area and materials

2.1 *Study area*

As is mentioned above, this study is concerned about the variation of wave characteristics in the Bohai Sea. The study area covers the Bohai Sea spanning between 37°–41°N and 117.5°–122.5°E (Fig. 1). As the only inner sea of China, attention to its wave characteristics and wave climate have been raised recently for a variety of reasons.

The Bohai Sea is a shallow semi-enclosed sea located in the northeast of China, which extends over an area of 77 000 km^2. It consists of the Liaodong Bay, Laizhou Bay, Bohai Bay, central shallow basin, and the Bohai Strait connecting with the outer Yellow sea. There are a number of platforms standing in the Bohai Sea constituting 20 drilling fields, and as the largest offshore oil drilling area in China, over 300 million tons of crude oil has been supplied since 1976 (Guo et al., 2019). Due to its special geographical position, which lied on the active zone at the edge of monsoon, the wind field conditions and the accompanying wave characteristics in this inner sea present complex changes with the long-term change of climate and the regional differences. However, few of the researches address this work in the sub-basins. In this context, the entire Bohai Sea is divided into five sub-sectors (shown in Fig. 1).

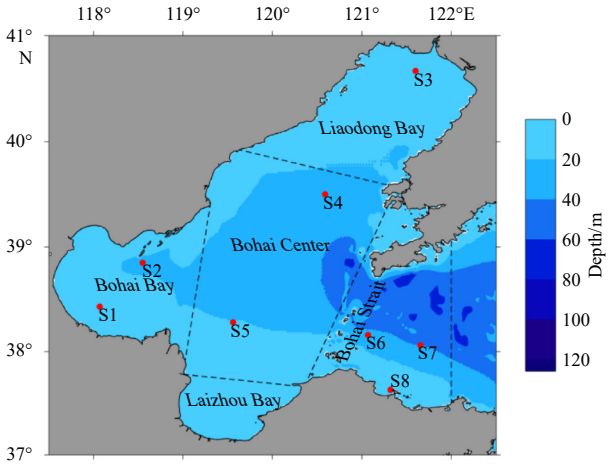

Fig. 1. Study area with ETOPO1 bathymetry. Regions partition by dashed lines and buoy locations used for validation are denoted by red dots.

2.2 *Dataset*

ERA5 is the fifth generation of atmospheric reanalysis produced by the European Centre for Medium-Range Weather Forecasts, which has used advanced modeling and data assimilation systems to combine numerous historical observations into global estimates (Hersbach et al., 2020). As the predecessor of ERA5, ERA-interim was widely applied to study the atmospheric, ocean and land physics and there is a lot of research on wave climate using ERA5 on a global or regional scale (Aboobacker and Shanas, 2018; Zheng et al., 2016; Dee et al., 2011).

Complete ERA5 (henceforth called ERA5) reanalysis released so far includes two products covering the period from 1979 onwards and the period from 1950 to 1978 (preliminary version), while the ERA5 BE (the product in 1950–1978) does not suffer from tropical cyclones (https://www.ecmwf.int/). The Copernicus Climate Change Service has retrieved the wave data in 0.5°×0.5° spatial resolution (Hersbach et al., 2020).

To quantitatively evaluate the applicability of the ERA5 wave datasets, eight buoys in different observation stations are selected to compare SWH of combined wave (C-SWH) from ERA5 reanalysis and the observations (Table 1), in which, S6–S8 are near the Bohai Strait, S4 and S5 situate in the Bohai Center, S1 and S2 locate in the Bohai Bay (Fig. 1) and S3 lies on the Liaodong Bay.

In addition, the data of buoy observations are all archived to the accordant time interval with the ERA5 dataset for comparat-

Table 1. Description of buoy locations

ID	Coordinates	Data available	Data source
S1	38.43°N, 118.07°E	2020. 01–2020. 12	China Meteorological Administration
S2	38.85°N, 118.55°E	2020. 01–2020. 12	China Meteorological Administration
S3	40.67°N, 121.60°E	2006. 08–2006. 09	Wang et al. (2010)
S4	39.60°N, 120.59°E	2018. 01–2019. 03	North China Sea Marine Forecasting Center of State Oceanic Administration
S5	38.28°N, 119.56°E	1996. 08–1996. 09	Wang et al. (2012)
S6	38.16°N, 121.07°E	2012. 04–2013. 02	China Meteorological Administration
S7	38.06°N, 121.65°E	2012. 04–2013. 01	China Meteorological Administration
S8	37.63°N, 121.32°E	2012. 04–2013. 01	China Meteorological Administration

ive analysis. The root means square error (RMSE), correlation coefficient (R) and the mean error (Bias) are calculated according to Eqs (1)–(3), respectively.

$$\mathrm{RMSE}=\sqrt{\frac{1}{n}\sum_{i=1}^{n}\left(y_i-x_i\right)^2}, \tag{1}$$

$$R=\frac{\sum_{i=1}^{n}\left(x_i-\bar{x}\right)\left(y_i-\bar{y}\right)}{\sum_{i=1}^{n}\left(x_i-\bar{x}\right)^2\sum_{i=1}^{n}\left(y_i-\bar{y}\right)^2}, \tag{2}$$

$$\mathrm{Bias}=\bar{y}-\bar{x}, \tag{3}$$

where n is the number of datapoints; x_i and y_i is the ith of the observations and ERA5 dataset; and $\bar{x}$ and $\bar{y}$ represents their mean value.

For each observation, the C-SWH of the nearest grid point from ERA5 is compared with that from the corresponding buoy. The correlation coefficient R is 0.84, the RMSE 0.30 and Bias 0.03, suggesting a good agreement amongst the ERA5 and the *in-situ* datasets.

3 Methodology

3.1 *Theil-Sen estimator*

Trend estimation can be conducted either by parametric or non-parametric methods, in addition, the parametric methods are applicable for the datasets which are independent and normally distributed while the nonparametric methods apply to the independent datasets. The Theil-Sen estimator is a non-parametric method for trend estimation, which selects the median slope among all lines for data pairs in the time series data (Sen, 1968; Theil, 1992). Compared to the simple linear regression, Theil-Sen estimator is a more robust method when fitting a line (Vanem and Walker, 2013).

A set of linear slopes for all pairs of datapoints $(t_i, y_i), i=1,\cdots,n$ is calculated as shown in Eq. (4),

$$T_k=\frac{y_j-y_i}{t_j-t_i},\ \text{for}\ k=1,\ 2,\cdots,N, \tag{4}$$

where t_i are discrete times; y_i are the wave parameter at t_i; N is the number of data pairs within the time series; and T_k is the slope of the $k_{\mathrm{th}i\text{-}j}$ pair $(j>i)$ in time series.

The Theil-Sen estimator is defined as the median of the slopes as shown in Eq. (5),

$$m=\begin{cases}T_{[(N+1)/2]}, & \text{for } N \text{ is odd}\\ \dfrac{T_{[N/2]}+T_{[(N+2)/2]}}{2}, & \text{for } N \text{ is even}\end{cases}, \tag{5}$$

which is also called Sen slope. The sign of m indicates the trend of the sample data, either increasing or decreasing, and its value represents the steepness of the trend. Then the intercept b can be set as the median of H_i-mt_i when m has been determined. Then the trend is determined on the form of $H_t=mt+b$. The confidence interval at a specific significance level k% for the slope estimation can be constructed to be the interval containing the middle k% of the slopes of lines for the pairs.

3.2 *Mann-Kendall test*

The Mann-Kendall test is a non-parametric test of randomness against trend, which generally used in hydrological and meteorological datasets to detect monotonic trends (Mann, 1945; Sen, 1968; Aydoğan and Ayat, 2018). For a null hypothesis of randomness, H_0, the wave height/wave period data in time series $[Y=(y_1,y_2,\cdots,y_n)]$ are n independent and identically distributed random samples. The alternative hypothesis, H_1, the test for trend is two-sided.

Based on the null hypothesis H_0, there is no trend. The test statistic, S can be defined as given in Eq. (6),

$$S=\sum_{i=1}^{n-1}\sum_{j=i+1}^{n}\mathrm{sgn}(y_j-y_i), \tag{6}$$

where n is the number of data points and sgn is the sign function which can be defined as given in Eq. (7),

$$\mathrm{sgn}\left(H_j-H_i\right)=\begin{cases}+1, & \left(H_j-H_i\right)>0\\ 0, & \left(H_j-H_i\right)=0\\ -1, & \left(H_j-H_i\right)<0\end{cases}. \tag{7}$$

For the assumption of the null hypothesis, S is symmetric and normally distributed, with a mean of zero and variance given in Eq. (8):

$$\mathrm{Var}\left(S\right)=n\left(n-1\right)\left(2n+5\right)/18. \tag{8}$$

And then the Z transformation is employed as shown in Eq. (9),

$$Z=\begin{cases}\dfrac{S-1}{\sqrt{\mathrm{Var}\left(S\right)}}, & S>0\\ 0, & S=0\\ \dfrac{S+1}{\sqrt{\mathrm{Var}\left(S\right)}}, & S<0\end{cases}. \tag{9}$$

Typically, a two-sided test is then performed by comparing the Z to the $\alpha/2$ percentage point of a standard normal distribution (Hirsch et al, 1982; Young and Ribal, 2019). For a given significance level, the null hypothesis, H_0 is unacceptable, that is, there is a statistically significant trend if $|Z|\geqslant Z_{1-\alpha/2}$. A positive/negative value of Z indicates an increasing/decreasing trend at the chosen significance level.

3.3 *FFNN*

In view of the 0.5°×0.5° spatial resolution of ERA5 reanalysis signifying almost 55 km in one bin, a FFNN is utilized to interpolate the wave parameter to a higher resolution. The similar manner to encrypt mesh is employed in Mahmoodi et al. (2019). basing on the spatial autocorrelation theory (Tobler, 1970; Goovaerts, 2000; Zhu et al., 2020), we assume that the spatial distribution of wave parameter information can be expressed as follows:

$$z_i=f(x_{i1},x_{i2},w_i,z_{j_1},z_{j_2},z_{j_3},z_{j_4},d_{ij_1},d_{ij_2},d_{ij_3},d_{ij_4}), \tag{10}$$

herein, z_i is the estimated value of the point to be predicted; x_i represents the location (longitude and latitude) of the estimated point; w_i is the water depth (from ETOPO1); z_{j_1}–z_{j_4} are the observed values of the 4 closest sample point; and d_{ij} is the distance from z_i and z_j.

In addition, for the wave parameters related to the wind, such as C-SWH, SWH of wind wave (SHWW), MWD of combined wave (C-MWD), MWD of wind wave (MDWW), MWP of combined wave (C-MWP) and MWP of wind wave (MPWW), the wind speeds in the closest spots extracting from the ERA5 reanalysis with 0.25°×0.25° spatial resolution are also considered as an argument.

Under this assumption, we take advantage of FFNN to approximate this nonlinear function, that is, the independent variables are taken as the input and the dependent variable is taken as the output neuron. In this work, we have used the grid data of 0.75°×0.75° resolution along with that of 0.5°×0.5° resolution to construct the training set, which includes training subset, validation subset and test subset. The network is trained taking advantage of gradient descent combined with the backpropagation technique. The other parameters and their values in FFNN are shown in Table 2. By applying the model after trained, data of interestedly higher resolution are achieved by adjusting the input dataset.

In this study, the original ERA5 data of 0.5°×0.5° spatial resolution are interpolated into that of 0.125°×0.125°. Figure 2 displays the points of ERA5 wave data (the dark dots with square pane) and the interpolated data (the blue dots) in the research region.

Table 2. The parameters and the corresponding values of the employed feedforward neural network

Parameter	Value
Training subset	0.6
Validation subset	0.2
Test subset	0.2
Number of hidden layer1 (L1) neurons	17
Number of hidden layer2 (L2) neurons	5
Learning rate	0.001
Momentum parameter	0.9
L2 regularization parameter	0.000 1
L1 activation function	hyperbolic tangent
L2 activation function	hyperbolic tangent
Output layer activation function	linear
Max iterations	3 000

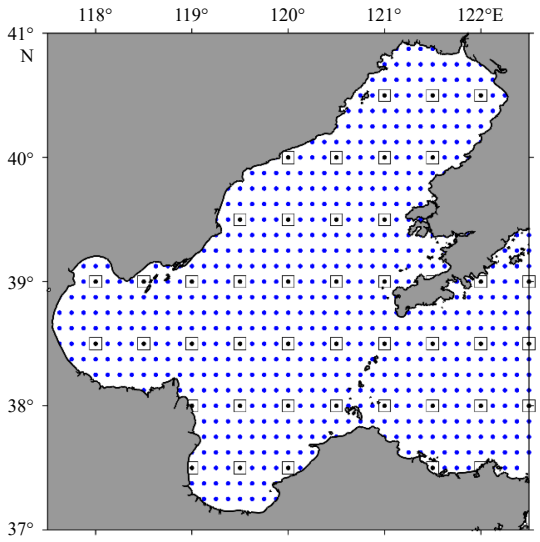

Fig. 2. ERA5 model (the black dots with square pane) and the interpolated (the blue) positions.

Moreover, the extended dataset is also validated against the *in-situ* buoys in the same manner to the original dataset. For the united data, R is 0.84 which shows the ERA5 data is of decently close association to the *in-situ* data. RMSE and Bias are 0.30 m and 0.02 m, individually. The resulting scatterplot is depicted in Fig. 3. Consequently, the extended ERA5 wave reanalysis can reflect the wave conditions over the whole Bohai Sea well.

The present study uses 71 years of hourly wave data including C-SWH, SHWW and SWH of total swell (SHTS), C-MWD, MDWW and MWD of total swell (MDTS), MWP, MPWW and MWP of total swell (MPTS) during 1950–2020 with 0.125°×0.125° spatial resolution.

Time series in the Bohai Sea are expected to present a strong seasonality (Lv et al., 2014). The inter-seasonal trends of the wave parameters are determined by the slope of simple linear regression and the Sen slope (Sen, 1968), the latter also called Theil-Sen estimator which have achieved good results in Aydoğan and Ayat (2018). Then the Mann-Kendall test (MK test), which is approved by the World Meteorological Organization for hydro-meteorological trend evaluation (Kundzewiz and Robson, 2000), performs to determine whether the resulting trends are statistically significant. In an identical manner, the tendencies of inter-annual variations and their significance are estimated. The influence from the decadal oscillations does not be taken into consideration in this paper, which may potentially impact the results.

4 Results and analysis

4.1 *Temporal variation of annual SWH*

Six time series are created by calculating the annual mean and 95th percentile values of all the interpolated ERA5 gridded C-SWH, SHWW and SHTS. The inter-annual variation of these time series under the mean and 95th percentile is then conducted by the Theil-Sen estimator and the simple linear regression. The confidence interval of the Sen slope and the confidence level of the MK test are set to 95% and 0.10, respectively.

Figure 4 shows the mean and the 95th percentile linear trends of C-SWH, SHWW and SHTS and the counterpart values are given in Table 3. In the tables and figures below, the simple linear regression, Sen slope and result based on MK test remark as b, T, and Z, respectively. The upper and lower confidence limits for Sen slope remark as $T\pm$CI. And the up/down arrow in tables means the positive/negative trend within a specified confidence limits for MK test, while the stub line stands for there is no signi-

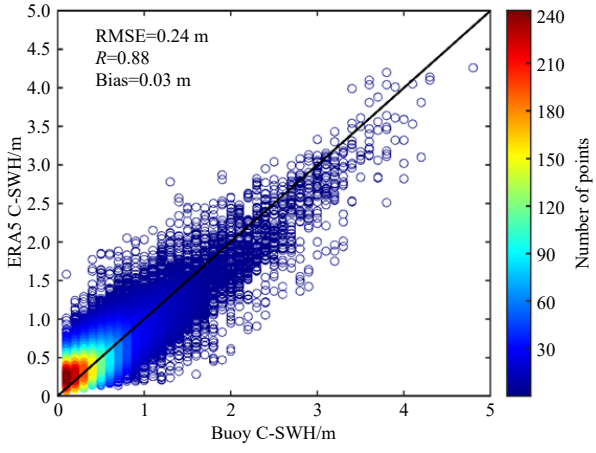

Fig. 3. The scatterplot between the extended ERA5 C-SWH and buoy C-SWH.

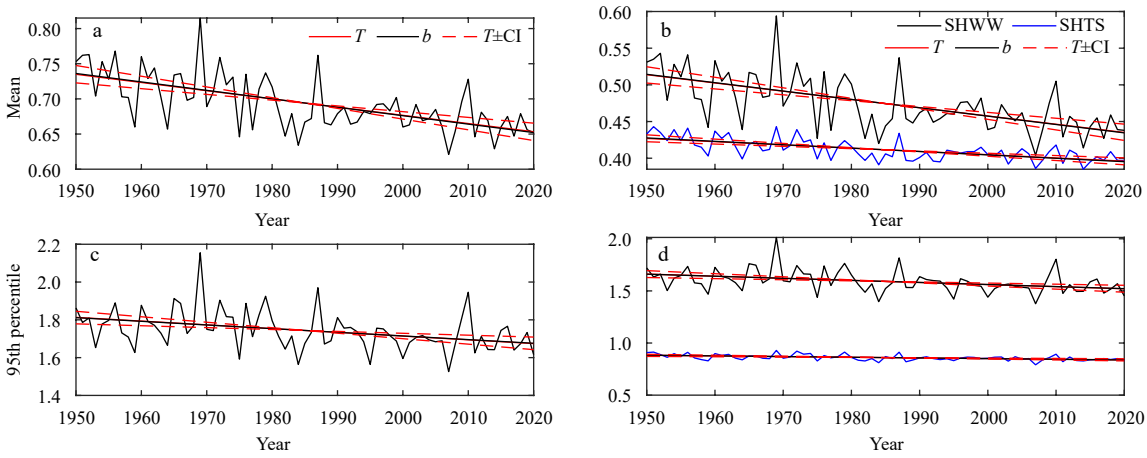

Fig. 4. Annual time series of mean (a, b) and 95th percentile (c, d) C-SWH (a, c), SHWW and SHTS (b, d) with their linear trend estimations in the whole Bohai Sea.

Table 3. The linear trends (cm/a) of inter-annual variation of C-SWH, SHWW and SHTS in the whole Bohai Sea within 90% confidence limits for MK test

Statistics	Wave height	*T*	*T*+CI	*T*–CI	*b*	*Z*	Trend
Mean	C-SWH	–0.12	–0.08	–0.15	–0.12	–5.41	↘
	SHWW	–0.11	–0.08	–0.14	–0.11	–5.26	↘
	SHTS	–0.04	–0.03	–0.06	–0.05	–5.63	↘
95th percentile	C-SWH	–0.20	–0.10	–0.29	–0.19	–3.59	↘
	SHWW	–0.20	–0.11	–0.30	–0.20	–3.78	↘
	SHTS	–0.06	–0.03	–0.09	–0.07	–3.99	↘

ficant trend for the tested time series.

Interestingly, the trends for all these situations mentioned above are negative whereas the wave height trends are positive in the majority of the world's oceans (Young and Ribal, 2019; Semedo et al., 2015). The result of trend estimation is in accordance with the previous research (Ren et al., 2017; Liu and Zhao, 2019), which shows annual mean SWH of combined wave decrease at rates of –0.30 cm/a and –0.85 cm/a in 1950–2011.

For the mixed wave, there is a decrease with rates of 0.12 cm/a and 0.20 cm/a for the mean and 95th percentile in the whole Bohai Sea. The mean trend is steeper and more significant than the 95th percentiles (Table 3), in which, the former's absolute *Z* is above 5 while the latter is less than 4. The difference reveals the mean wave state seems to be affected more by the climate change in comparison to the extreme one.

For the wind wave and swell, the trajectory of SHWW is always above the SHTS one, indicating that the entire Bohai Sea is wind wave dominated. The decreasing trend of SHWW is more obvious than that of SWTS and both its *T* and *b* are much larger, while the swell is gentler but more significant. Thus, the negative trend of the overall C-SWHs is mainly due to the obvious decrease of the wind wave. Additionally, the results from Sen slope and the slope of simple linear regression are equivalent, their difference in the two pair of trends above are approximately 0.01 cm/a. This reveals the simple linear regression provides the similar result compared to the Theil-Sen estimator, though it is known as a crude trend estimation approach (Vanem and Walker, 2013; Aydoğan and Ayat, 2018).

4.2 *Temporal variation of seasonal SWH*

Since the East China Sea located in the most typical monsoon climate region over the world, the Northwest Pacific Ocean, the development and change of monsoon determines the wave variations in this sea area. In the following part, the inter-seasonal trend of SWH is evaluated. Differ from the other research (Ren et al., 2017; Lv et al., 2014), this paper has taken a more detailed way to show the seasonal variation by analyzing each month separately. The results under two different statistics (mean and 95th percentile) are discussed in the two following sub-sections.

4.2.1 *Mean trend*

The monthly change of the mean C-SWH, SHWW and SHTS are given in Fig. 5 and Table 4, which the C-SWH are figured in the subplot marked "a" and SHWW and SHTS are in "b".

Figure 5a and the left part of Table 4 show that January, February, June, July, August and September have significantly negative trends and the rest have no clear trend within 90% confidence limit from MK test. The months tested to be effective are mostly in summer (June, July and August) and winter (December, January and February). Hence, the negative trend in annual C-SWH can be primarily attributed to the decrease in summer and winter. The largest decrease occurs in February with –0.24 cm/a and –0.26 cm/a of *T* and *b* respectively and the most significant trend is in September whose absolute value of *Z* reaches up to 3.93.

Figure 5b depicts that the monthly average SHWWs are generally higher than SHTSs. But for the months in summer, particularly in June, the result is opposite illustrating that the wind wave is weaker in summer than in winter. According to Table 4, the trends of the SHWW and SHTS are same for most months, which is also same to that of C-SWH. SHWW decrease ranging from –0.03 cm/a to 0.23 cm/a with an average value of –0.16 cm/a in winter and –0.12 cm/a in summer. SHTS decrease ranging from –0.00 cm/a to 0.09 cm/a with an average value of –0.07 cm/a in winter and in summer. The largest decrease is –0.23cm/a for mean SHWW and –0.09 cm/a for mean SHTS, both occurs in

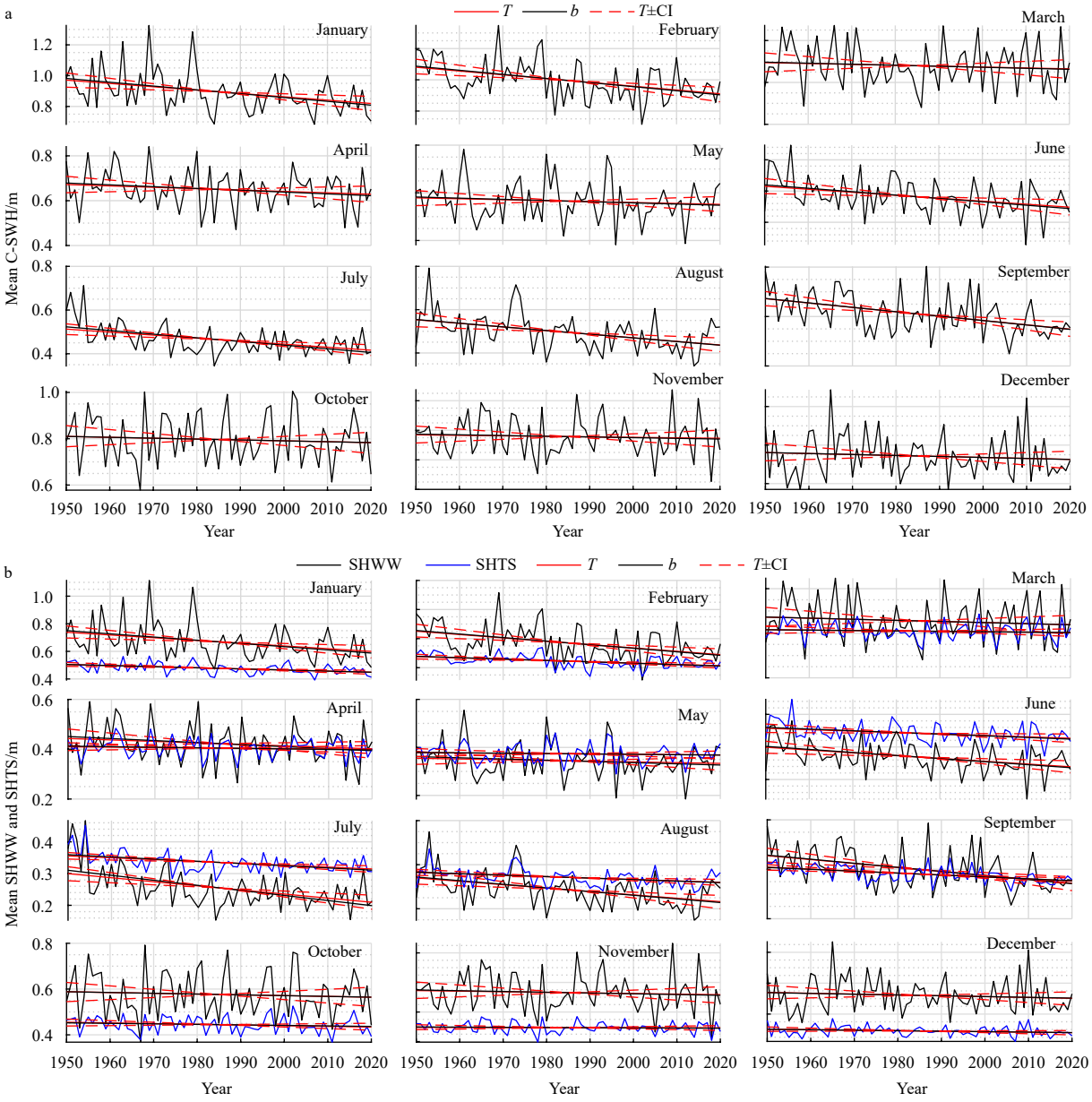

Fig. 5. Mean trend in monthly C-SWH (a), SHWW and SHTS (b) over the period of 1950–2020 in the whole Bohai Sea.

Table 4. The mean trends (cm/a) of monthly variation of C-SWH, SHWW and SHTS in the whole Bohai Sea within 90% confidence limits for MK test

Month	C-SWH				SHWW (SHTS)			
	b	*T*	*Z*	Trend	*b*	*T*	*Z*	Trend
January	−0.25	−0.22	−3.22	↘	−0.23 (−0.08)	−0.20 (−0.08)	−3.12 (−3.64)	↘ (↘)
February	−0.26	−0.24	−3.48	↘	0.24 (−0.10)	−0.23 (−0.09)	−3.60 (−3.53)	↘ (↘)
March	−0.05	−0.04	−0.65	–	−0.05 (−0.02)	−0.05 (−0.02)	−0.82 (−0.70)	–(–)
April	−0.08	−0.06	−1.10	–	−0.08 (−0.02)	−0.06 (−0.01)	−1.40 (−0.39)	↘ (–)
May	−0.05	−0.04	−0.71	–	−0.05 (−0.02)	−0.03 (−0.01)	−0.66 (−0.66)	–(–)
June	−0.11	−0.10	−2.95	↘	−0.09 (−0.05)	−0.09 (−0.04)	−3.24 (−2.43)	↘ (↘)
July	−0.17	−0.14	−3.81	↘	−0.16 (−0.07)	−0.13 (−0.06)	−4.00 (−3.71)	↘ (↘)
August	−0.17	−0.17	−3.53	↘	−0.17 (−0.07)	−0.15 (−0.06)	−3.66 (−3.29)	↘ (↘)
September	−0.18	−0.18	−3.93	↘	−0.17 (−0.08)	−0.16 (−0.08)	−3.92 (−4.32)	↘ (↘)
October	−0.04	−0.04	−0.57	–	−0.03 (−0.02)	−0.03 (−0.03)	−0.45 (−1.15)	–(–)
November	−0.05	−0.03	−0.46	–	−0.05 (−0.01)	−0.04 (−0.00)	−0.55 (−0.19)	–(–)
December	−0.05	−0.05	−0.89	–	−0.05 (−0.03)	−0.05 (−0.03)	−0.92 (−1.52)	–(↘)

February. The SHTS shows a gentler variation over this 71-year long period contrast with SHWW considering its values of the slope are smaller and the time series are milder (Table 4). This result suggests that the significant decrease of C-SWH is more likely due to the dramatic reduction from wind wave resulting from the weakening of the summer and winter monsoon in this area (Ding et al., 2008; Kang et al., 2018).

In fall (September, October and November) and spring (March, April and May), which both are transition period between summer monsoon period and winter monsoon period, SWHs appear to diminish in a slighter extent (except for September) with an unsignificant trend. Again, for all months both the simple linear regression and the Theil-Sen estimator give the same result of the long-term trend, either increasing or decreasing.

4.2.2 *95th percentile trend*

The upper (95th) percentile seasonal trend is given in Fig. 6 and Table 5. Similar to the mean case, the general variation in all months is also estimated to be negative, which is consistent with the annual results.

Figure 6a and the left part of Table 5 show October and December have positive tendency of the trend derived from both the simple linear regression and Theil-Sen estimator, yet tested to be ineffective. January is the month that C-SWH decreased the most and June is the most significant. 95th percentile C-SWH is decreasing effectively in January, February, April, June, July, August and September, which is practically identical to the mean situation expect for April. The consequence of the same effective months demonstrates that the decrease of C-SWH in the Bohai Sea is triggered by the decrease in summer and winter.

As listed in Table 5, the highest negative trend is in January for 95th percentile SWH of combined wave with rates of –0.48 cm/a for combined wave, –0.47 cm/a for wind wave and –0.15 cm/a for swell.

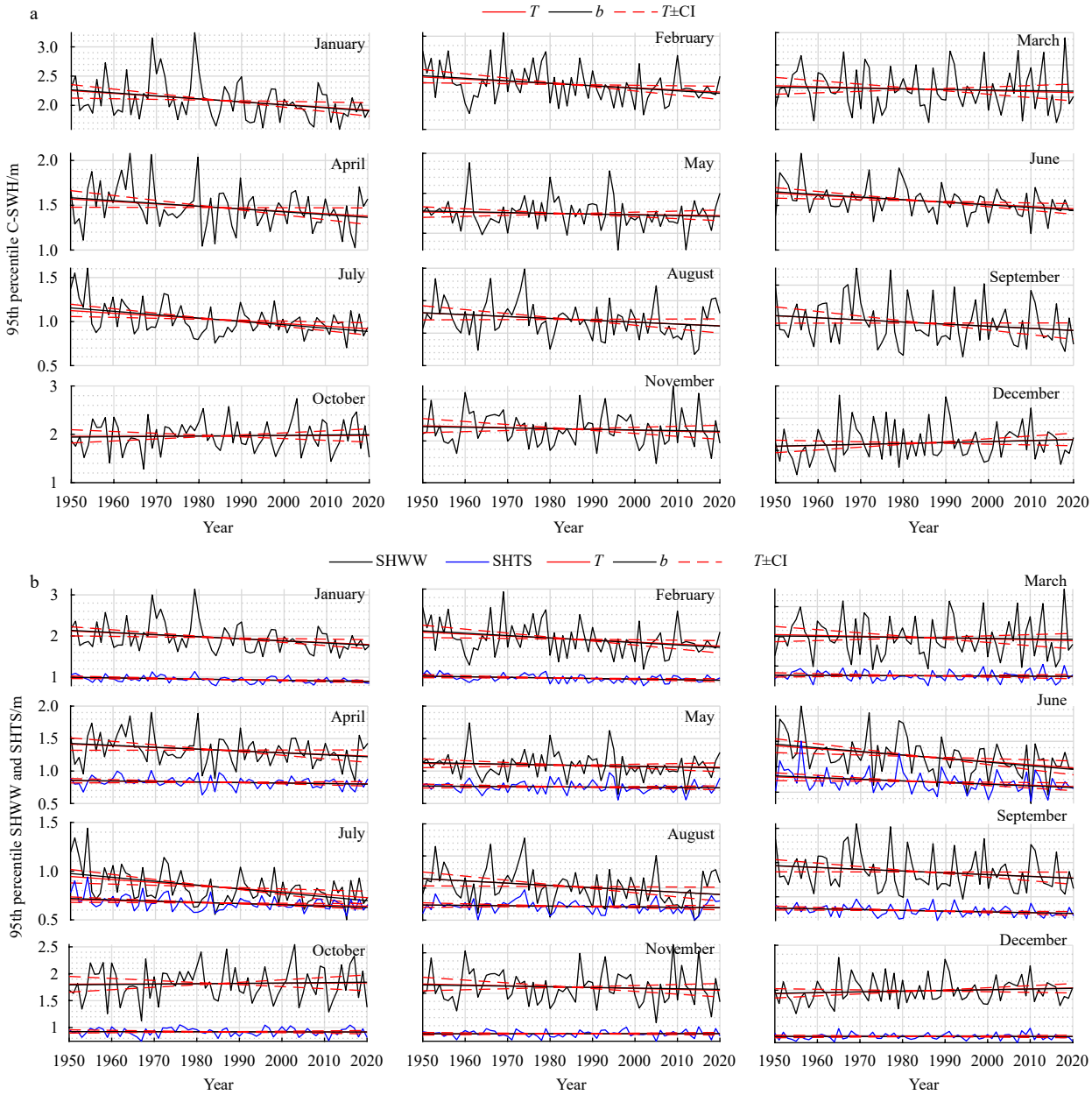

Fig. 6. 95th percentile trend in monthly C-SWH (a), SHWW and SHTS (b) over the period of 1950–2020 in the whole Bohai Sea.

Table 5. The 95th percentile trends (cm/a) of monthly variation of C-SWH, SHWW and SHTS in the whole Bohai Sea within 90% confidence limits for MK test

Month	C-SWH				SHWW (SHTS)			
	b	*T*	*Z*	Trend	*b*	*T*	*Z*	Trend
January	−0.52	−0.48	−2.69	↘	−0.51 (−0.15)	−0.47 (−0.15)	−2.70 (−3.22)	↘ (↘)
February	−0.54	−0.46	−2.50	↘	−0.55 (−0.14)	−0.47 (−0.13)	−2.41 (−2.60)	↘ (↘)
March	−0.09	−0.15	−0.89	–	−0.08 (−0.02)	−0.15 (−0.04)	−0.81 (−0.81)	– (–)
April	−0.31	−0.27	−2.04	↘	−0.29 (−0.08)	−0.26 (−0.07)	−1.91 (−1.32)	↘ (↘)
May	−0.10	−0.06	−0.63	–	−0.12 (−0.04)	−0.08 (−0.04)	−0.82 (−0.96)	– (–)
June	−0.29	−0.25	−2.98	↘	−0.28 (−0.13)	−0.25 (−0.11)	−3.00 (−2.43)	↘ (↘)
July	−0.38	−0.29	−2.87	↘	−0.40 (−0.13)	−0.31 (−0.09)	−3.28 (−2.32)	↘ (↘)
August	−0.29	−0.28	−1.84	↘	−0.35 (−0.06)	−0.35 (−0.06)	−2.12 (−1.11)	↘ (–)
September	−0.26	−0.26	−1.91	↘	−0.26 (−0.11)	−0.25 (−0.11)	−1.97 (−2.63)	↘ (↘)
October	0.07	0.03	0.11	–	0.07 (−0.01)	0.03 (−0.01)	0.19 (−0.24)	– (–)
November	−0.16	−0.22	−0.89	–	−0.16 (0.01)	−0.22 (0.00)	−0.94 (0.07)	– (–)
December	0.14	0.15	1.04	–	0.16 (−0.00)	0.18 (0.00)	1.09 (−0.03)	– (–)

The time series depicted in Fig. 6b show that the wind wave is stronger than the swell in extreme wave state for all months. Combined with Fig. 5b, the swell is more stable with a smaller amplitude, and its wave heights are in the range of 0.2–1.0 m. The difference that the absolute values of *T* are larger than the mean case while those of *Z* are smaller indicates that although the 95th percentile C-SWH has a steeper decrease, the trend takes smaller significance. Besides, the wave heights in winter are the largest, followed by fall, spring and summer minimum.

4.3 *Spatial distribution of SWH*

In the following part of this context, spatial distribution of long-term SWH is analyzed by showing the heatmap. Both the value and the trend are discussed in this part showing the obvious region difference through this shallow basin. The heatmap is in 0.5°×0.5° spatial resolution realized by calculating the mean/95th percentile SWH from the 0.125°×0.125° grid.

The heatmap charts of the spatial distribution of the mean and 95th percentile C-SWHs, SHWWs and SHTSs from 1950 to 2020 are shown in Fig. 7. The resemblance between the two pairs of graphs is that the values of SWH is larger in the southern Bohai Center and the intersecting zone of the Bohai Sea and Yellow Sea, while relatively small near the shore.

From the middle and right panel in Fig. 7, the spatial distribution of SHWW and SWTS both show strong regional differences. SHWWs' numerical difference is more apparent, particularly in 95th percentile case, which varies from 3.11 to 0.87. While for the SHTS, the difference of maximum and the minimum is 0.70 (1.28–0.58). This reveals the result in uniformity with the conclusion stated before (the swell is gentler).

Under severe conditions, the larger value of SHWW appears in the Liaodong Bay and the intersection of the Bohai Sea and Yellow Sea, which is close to the location of the Bohai Sea's gale belt. Different from wind wave, the largest SWTS occurs in the intersection of Laizhou Bay and the Bohai Sea and Yellow Sea, which is resemble to the large swell area of the Bohai Sea.

4.3.1 *Inter-annual trend*

Informed by the second part of this chapter, the negative trends over 6 months are checked to be not significant within the 90% limits of the MK test. To get a better understanding of the distributions of the negative trends in the Bohai Sea, we use the

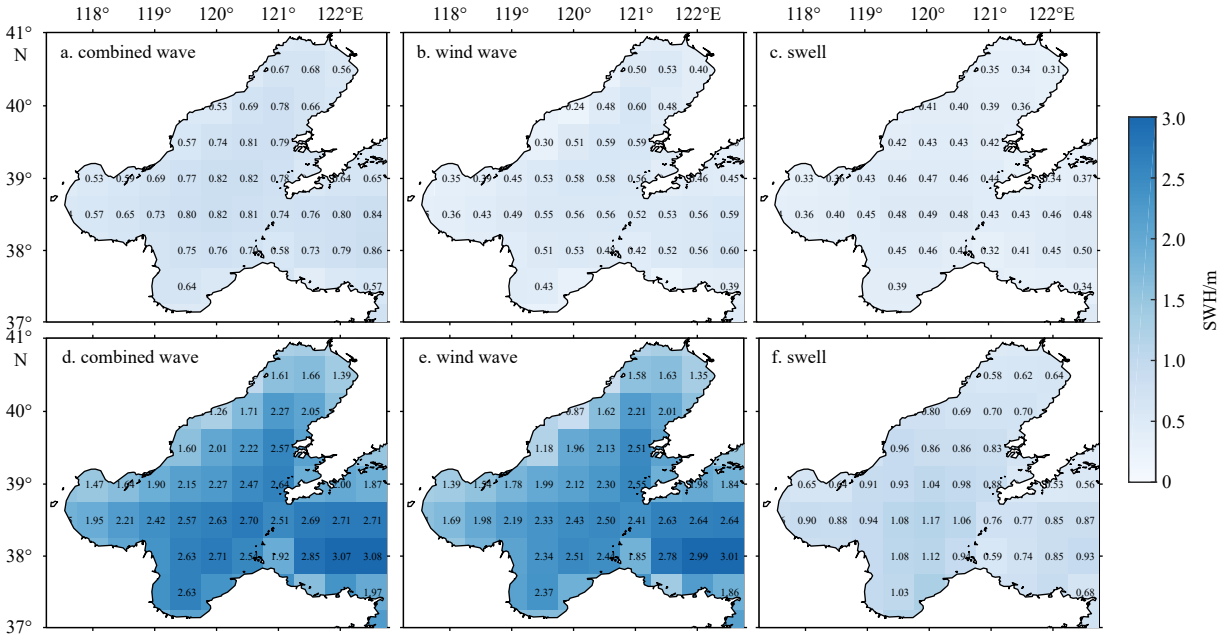

Fig. 7. Heatmaps of spatial distribution in mean (a–c) and 95th percentile (d–f) C-SWH (a, d), SHWW (b, e) and SHTS (c, f).

approach employed in Aydoğan and Ayat (2018) to illustrate the confidence level of each trend without a specified a threshold for MK test, and the trend will be considered to be unacceptable if the confidence level is less than 0.5.

The analysis followed focuses on that of combined wave, which is more informative, and the spanning period is 1950–2020 in both cases. The spatial distributions of the inter-annual trends in the mean and 95th percentile C-SWH are mapped at the top of Fig. 8 and the corresponding confidence levels are depicted below them.

The overall mean SWHs in the Bohai Sea shows a negative trend. The regional variability of T value as depicted in Fig. 8 (left row) is similar to the wave height in mean case. The negative value of Sen slope for monthly mean C-SWH is highest in the Bohai Center and decreases as closer to shore in Bays. The corresponding confidence levels, which in all the sectors are high up to over 98%, reveal the negative trends are of great significance. In the east of Bohai Strait, connecting with the Yellow Sea, the decreasing trend have a rather lower values and the significances are also rather lower than the inner of this semi-closed sea.

In the 95th percentile case, there are some positive T values derived from Theil-Sen estimator in the southeastern Bohai Sea (contains part of Bohai Center and Bohai Strait), which are much higher in the intersection of the Bohai Sea and Yellow Sea. But it is evident that they are not significant as a result of their corresponding confidence level is smaller than 50%. The higher T values occur in the Bohai Bay and Liaodong Bay.

4.3.2 *Inter-seasonal trend*

The similar fashion to Section 3.3 is conducted for each month to display the inter-seasonal variation. The heatmaps of the Sen slope and the confidence levels for mean C-SWHs representing the average sea state are mapped in Figs 9 and 10. Figures 11 and 12 show the trends of 95th percentile C-SWHs standing for the extreme sea state.

The distribution of mean trend also demonstrates a strong seasonality (see Fig. 9). C-SWH decreases the most with rate of −0.35 cm/a in the belt from the western Liaodong Peninsula to the Laizhou Bay in January. In February, which second highest negative trend occurs in a year, the wave heights decrease more in the southeastern Bohai Sea in the Laizhou Bay and between the Bohai Bay and Bohai Center. In summer, negative trend varies from −0.03 cm/a to −0.22 cm/a and is steeper from the Liaodong Bay to the Bohai Bay. The decreasing rates in spring and fall is comparable for each month, which are higher in offshore region. September has a lower variation among regions for Sen slope, ranging in −0.08–−0.19 cm/a.

As mapped in Fig. 10, the months which tested to be not significant in Section 4.2.1 possess the bins of an unacceptable confidence level or have most bins of lower confidence levels. It is the intersection of the Bohai Sea and the Yellow Sea that the trend is most not significant, and the majority of the bins show an intolerable result. Generally, the higher increasing rates are tested to be less significance.

The ratios of the Sen slope in extreme sea station are sharper than the mean one as a consequence of the larger T and deeper colors in the heatmaps shown in Fig. 11. As is noted before, the trends in spring and fall are inconspicuous. In comparison with the mean trend, the spatial distribution in February–October is similar, while there are much more bins of negative trends in

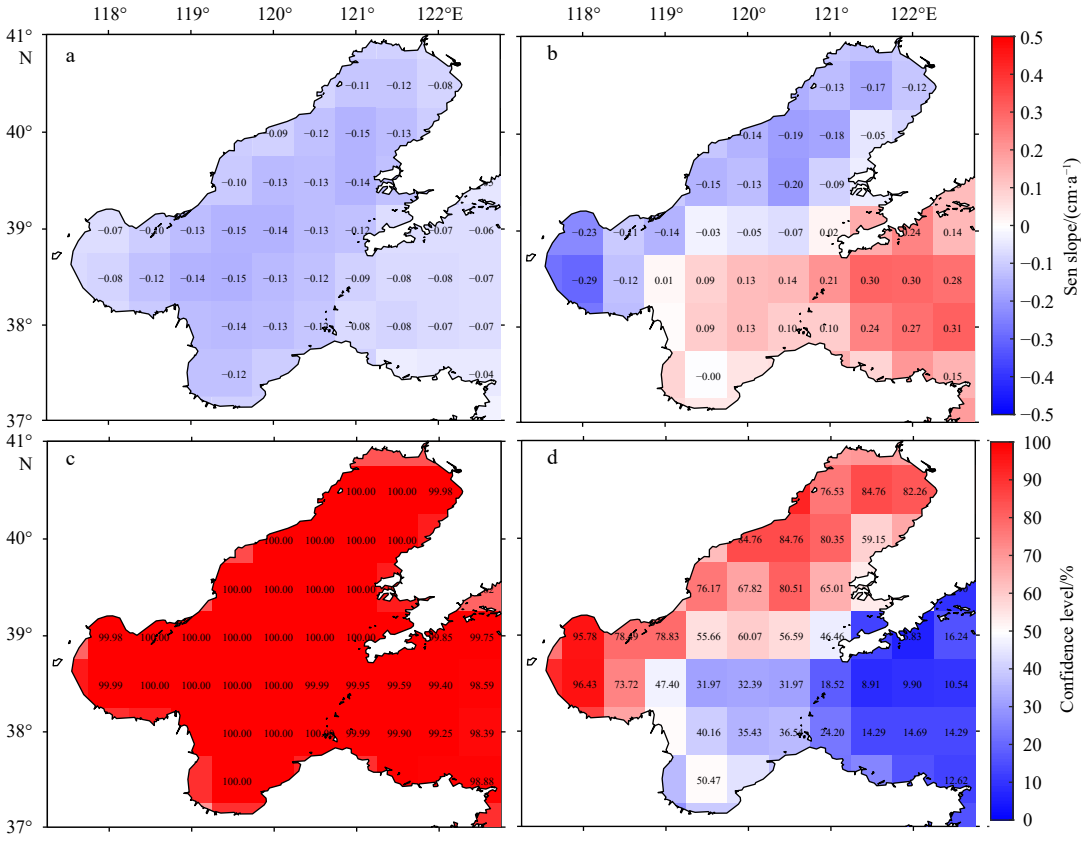

Fig. 8. Heatmaps of inter-annual trend (a, b) and confidence levels (c, d) in mean (a, c) and 95th percentile C-SWH (b, d).

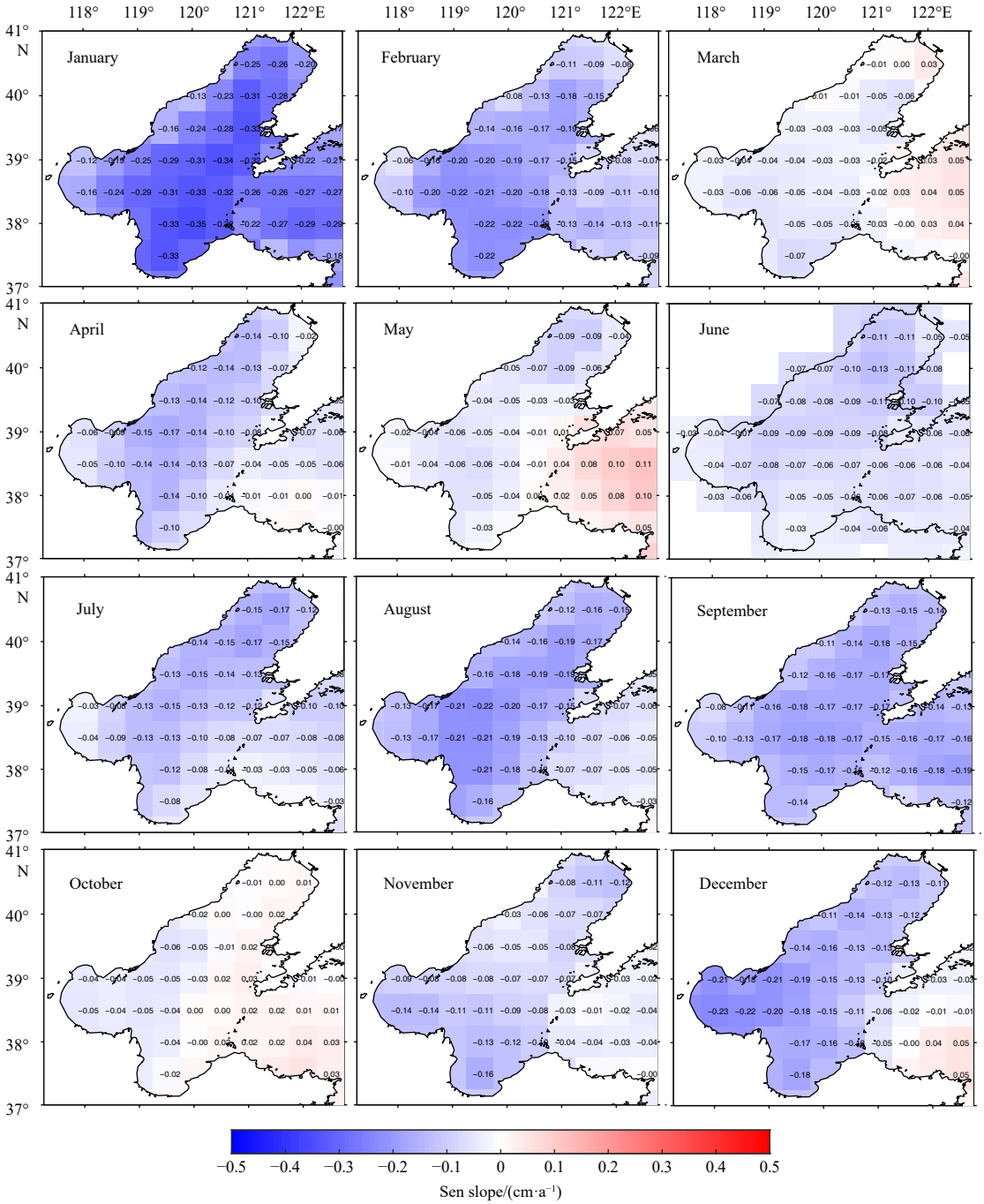

Fig. 9. Heatmaps of inter-seasonal trend in mean C-SWH for each month.

November (Fig. 11) and a number of bins owning positive trends in December (certainly not significant). In January, the major decrease centralizes in the Laizhou Bay and Bohai Bay.

It is distinct that in the 95th percentile case (Fig. 12), unlike the mentioned situation before, almost all the sub-heatmaps contain the unacceptable bins and they are also existed even in the months in summer. The months whose heatmap reveals a more significant trend are January, April, September and November.

4.4 *Wave direction and wave period*

4.4.1 *Seasonal prevailing wave direction*

For the purpose of analyzing the wave directions in the Bohai Sea, the frequencies of each wave direction in terms of wind wave, swell and combined wave are calculated. Table 6 shows the seasonal dominant wave direction associated with the frequency for the whole Bohai Sea. On the basic of the region partition (as displayed in Fig. 1), seasonal wave directions for separated wave fields are shown in Fig. 13. Located in the East Asian monsoon region, the waves in the Bohai Sea performs highly related with the monsoon. There is mainly southerly monsoon prevails in summer and north monsoon in winter.

In summer, the 1st and 2nd dominant wave direction for combined wave is S and SSE, respectively, with frequency of 17.66 and 15.65; for wind wave, it is SSE and S with frequency of 16.64 and 15.67; for swell, it is NE and S with frequency of 27.12

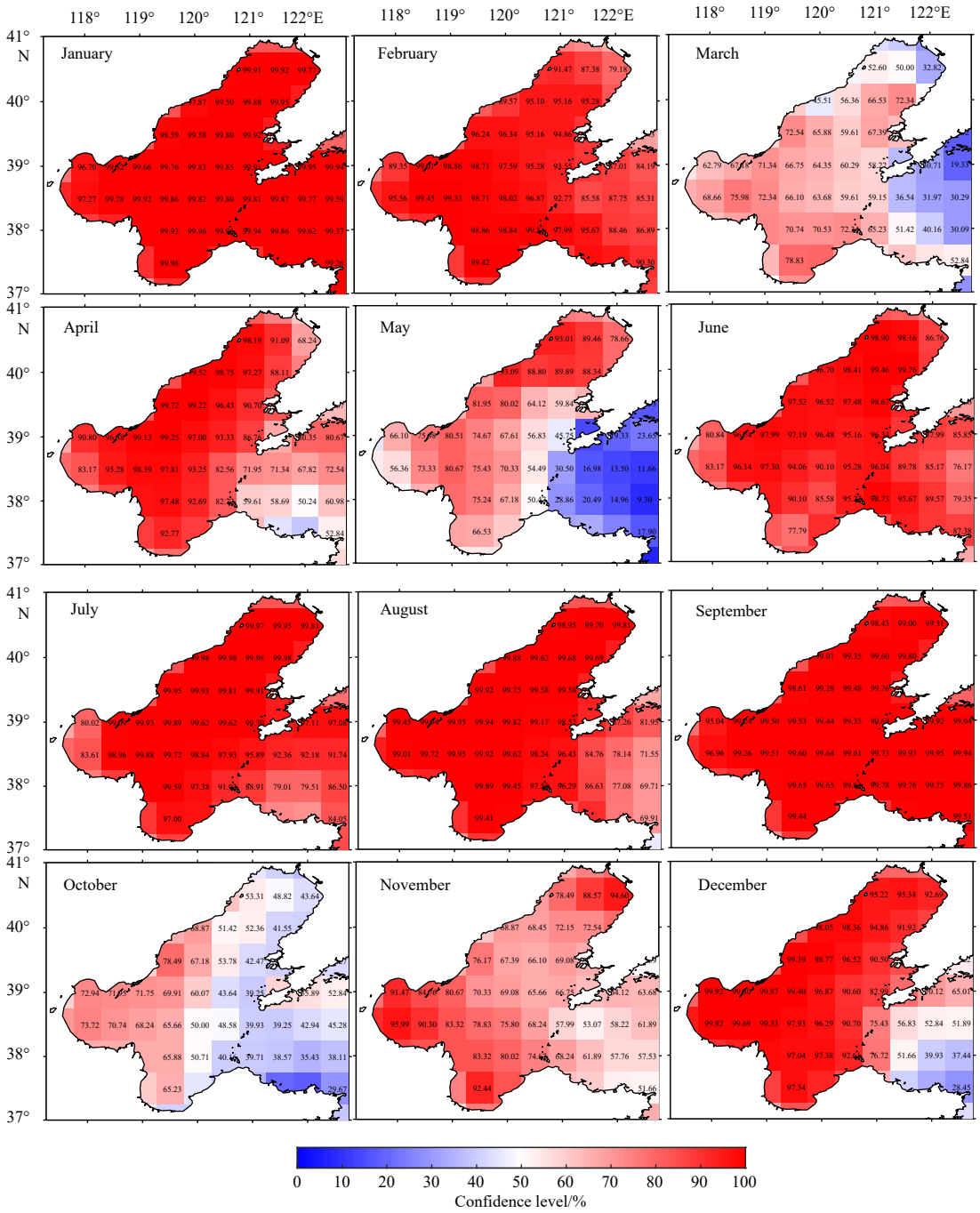

Fig. 10. Spatial distribution of the mean C-SWH inter-annual variation.

and 11.74. With the impact of the monsoon, wave direction of combined wave and wind wave are almost consistent. In the period of winter monsoon, the waves from NNE and N are dominant for combined wave and wind wave. Spring and fall are the interim seasons between the winter monsoon and summer monsoon season. As shown in Table 6, the distribution of dominant wave directions in spring is similar to that in summer, and that in fall is similar to that in winter.

It is clear from the Fig. 13 that the wave directions have a distinct disparity among the regions in the Bohai Sea. The distribution of MWD in each sub-sector is greatly different, which in the Bohai center is the most similar in comparison with the whole Bohai Sea. For this semi-enclosed sea, MDTS shows a great resemblance between all seasons, which is the wave of NE prevails.

4.4.2 *Annual trend analysis for MWP*

Same to the SWH, the trend analysis and test are carried for the MWP. The annual trend of basin MWP estimated by simple linear regression and Theil-Sen estimator with Mann-Kendall test is displayed in the Fig. 14. Also, the long-term trends of annual SWH in terms of combined wave, wind wave and swell are shown along with the 95% confidence interval of slope.

Figure 14 illustrates a rather similar trend to the SWH, especially for that of combined wave. The annual mean trends for MWP are all negative, with Sen slope of –0.17 for combined wave, –0.13 for wind wave and –0.24 for swell, which are tested to be

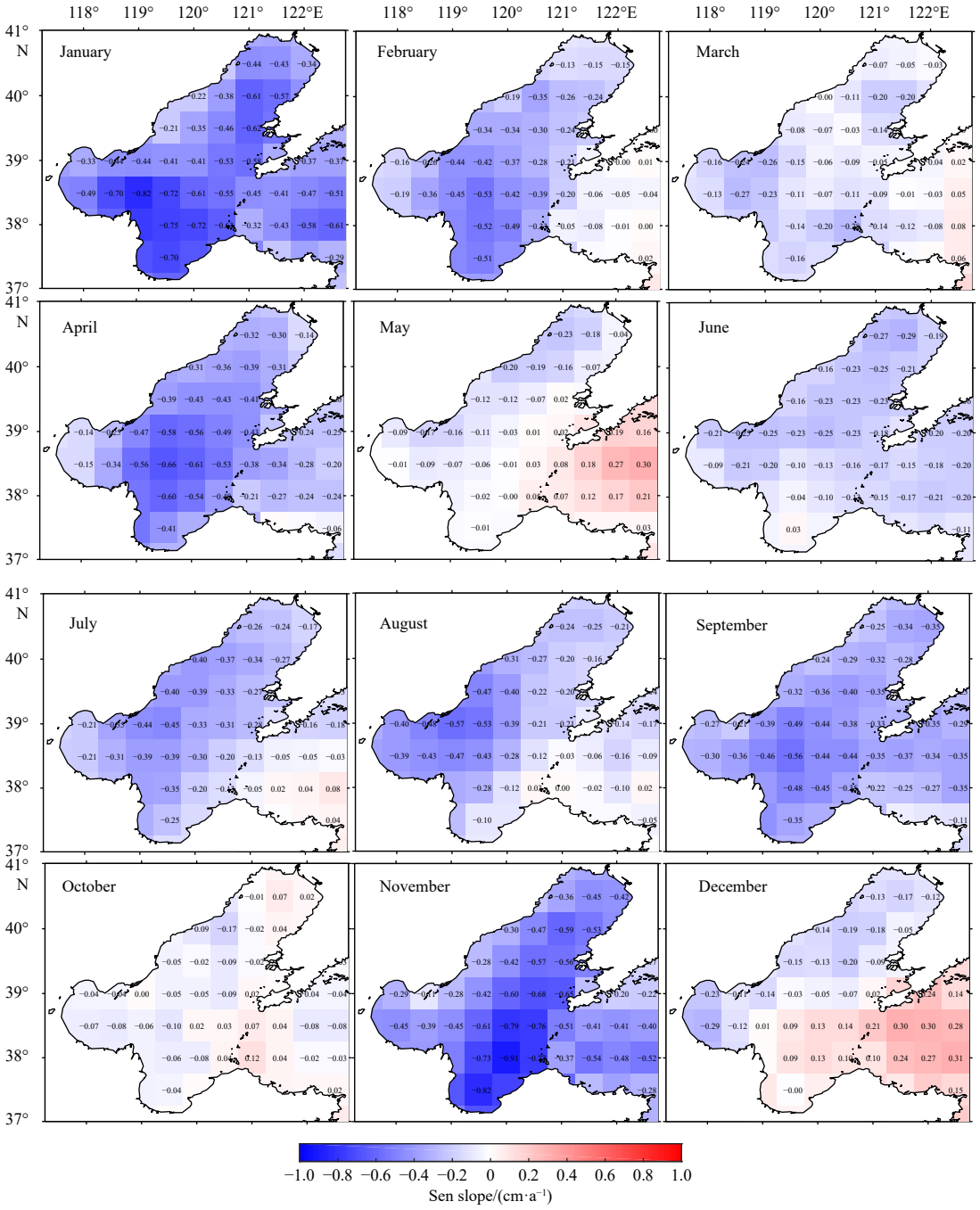

Fig. 11. Heatmaps of inter-seasonal trend in 95th percentile C-SWH for each month.

significant by Mann-Kendall test. In the case of 95th percentile, long-term trend derived from Theil-Sen estimator decreases with −0.16 s/a for C-MWP, −0.30 s/a for MPWW and −0.24 s/a for MPTS. Figure 15 shows the spatial variability of inter-annual trend and significance for C-MWP.

The averaged C-MWP during this long period significantly decreases covering almost all grids. For extreme wave state, there are several grids with positive Sen slope in south of Bohai Sea, yet tested to be not effective. That is, the long-term trend of C-MWP is also generally negative.

5 Conclusions

In summary, this study has taken advantage of an artificial intelligence method, FFNN, to interpolate the ERA5 reanalysis to the fine grid in the Bohai Sea, and presented the spatiotemporal variations of wave parameters based on the 71-year (1950–2020) interpolated ERA5 dataset.

The long-term trend analysis of SWH has a great reference value for engineering applications. This study has mainly focused on the long-term variability of SWH in terms of combined wave, wind wave and swell guided by the Theil-Sen estimator combining with the Mann-Kendall test.

Annually C-SWHs decrease with rates of –0.12 cm/a and –0.20 cm/a for the mean and the 95th percentile from 1950 to 2020 in the Bohai Sea. The inter-seasonal analysis shows the long-term term of SWH have strong seasonality, and SWH de-

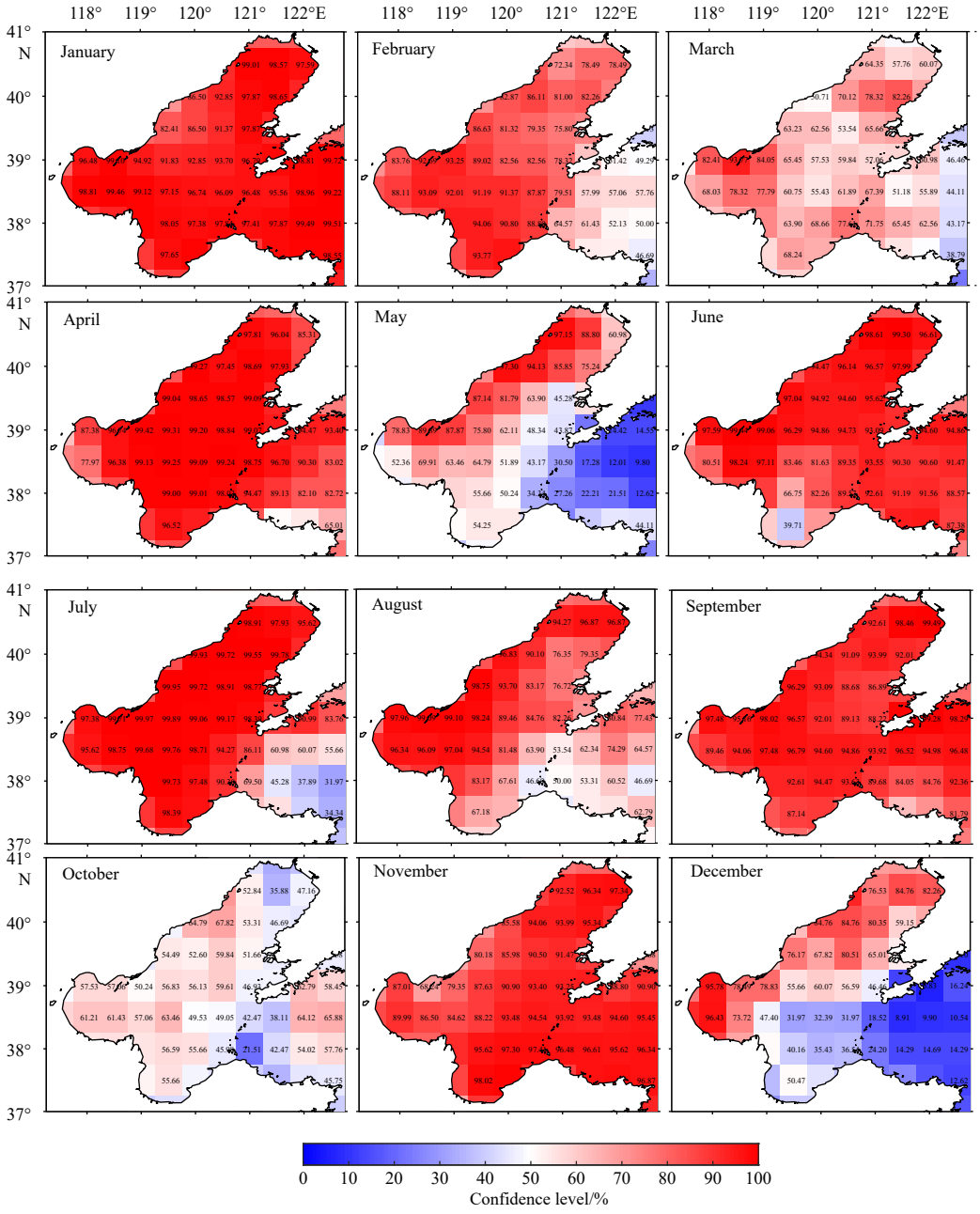

Fig. 12. Spatial distribution of the 95th percentile C-SWH inter-annual variation.

Table 6. The seasonal 1st and 2nd dominant wave direction and frequency (%) for the whole Bohai Sea over 1950–2020

			Spring	Summer	Autumn	Winter
Combined wave	Dominant	Wave direction	SSW	S	NNE	NNE
		Frequency/%	13.90	17.66	13.83	14.68
	Secondary	Wave direction	S	SSE	NE	N
		Frequency/%	13.70	15.65	10.00	14.01
Wind wave	Dominant	Wave direction	S	SSE	NNE	NNE
		Frequency/%	12.38	16.64	12.24	15.65
	Secondary	Wave direction	SSW	S	NE	N
		Frequency/%	11.39	15.67	10.42	11.63
Swell	Dominant	Wave direction	NE	NE	S	SSE
		Frequency/%	22.02	27.12	12.38	16.64
	Secondary	Wave direction	SSW	S	SSW	S
		Frequency/%	11.36	11.74	11.39	15.67

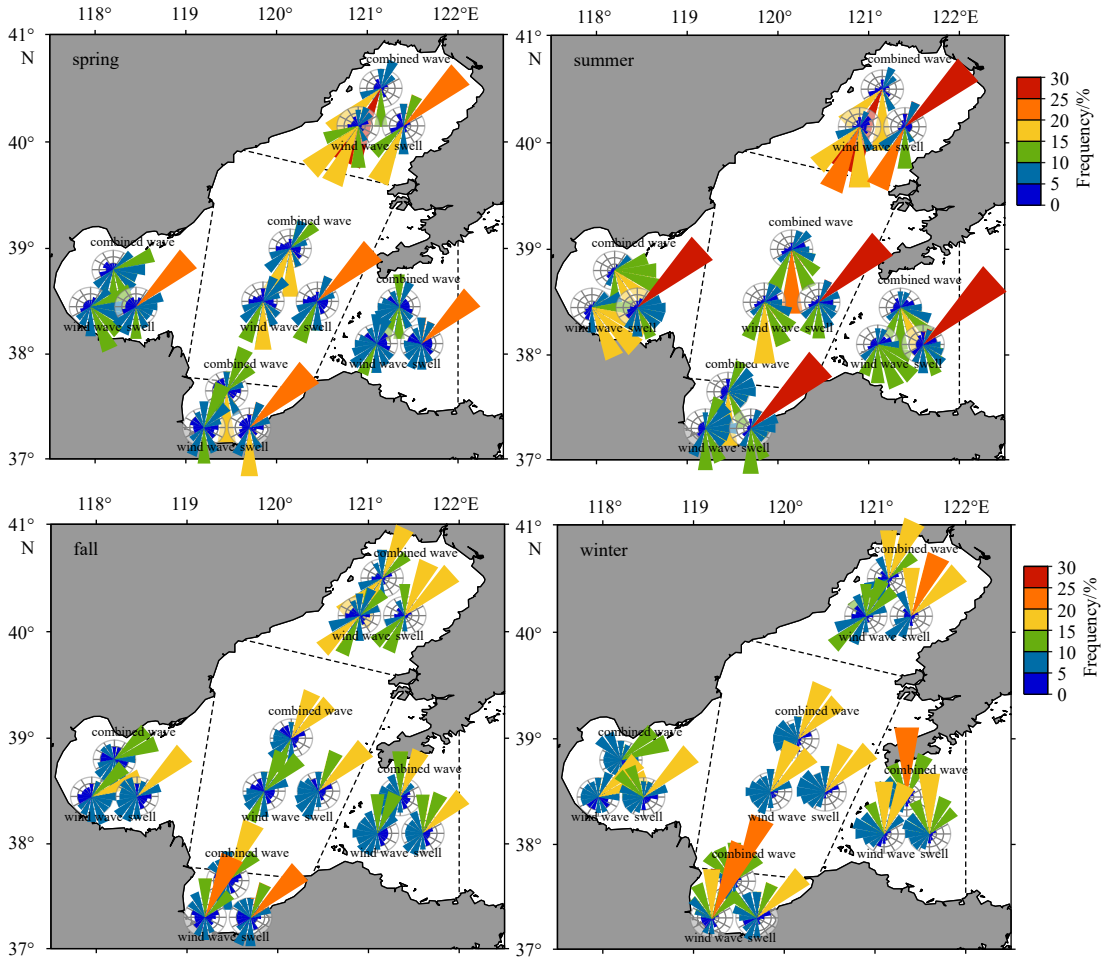

Fig. 13. The box plot of mean wave period during 1950–2020.

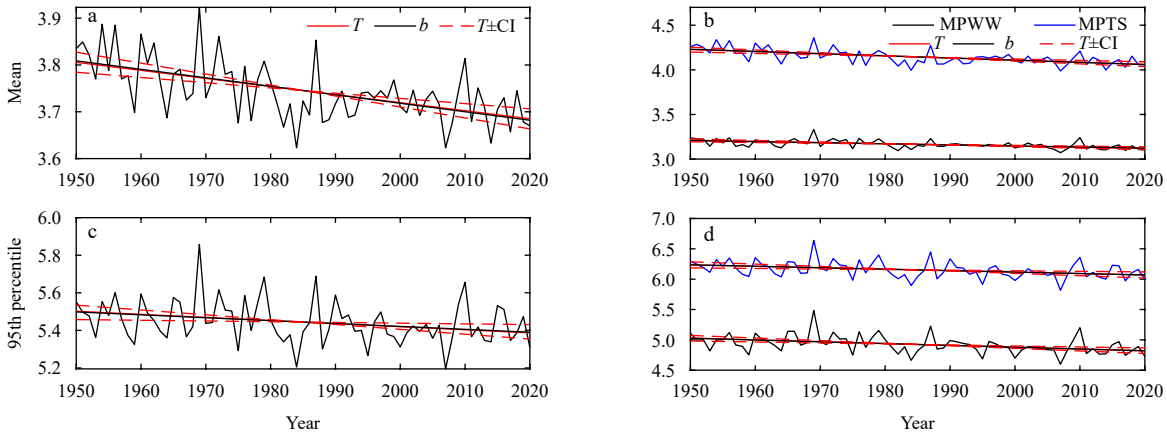

Fig. 14. Annual time series of mean (a, b) /95th percentile (c, d) C-MWP (a, c), MPWW and MPTS (b, d) with their linear trend estimations.

creases more in January, February, June–August and September. The spatial variations for the trend in the mean and severe sea states reflecting by mean and 95th percentile SWH are both obvious, and the negative trend concentrates on the inner Bohai Sea with higher values in offshore bays. The decreasing trend for annually C-SWH is probably owing to the weakening of winter and summer monsoon in this area as that the negative Sen slopes of wind wave are higher than swell especially during the months in summer and winter. The value of negative trend is –0.11 cm/a for annually mean SHWW and –0.04 cm/a for SHTS.

Consist with the monsoon, the dominant wave direction in spring and summer is nearly south, while in winter and fall it is nearly north. The seasonal variability of wave directions for mixed wave fields is closer to that for wind wave. The annual

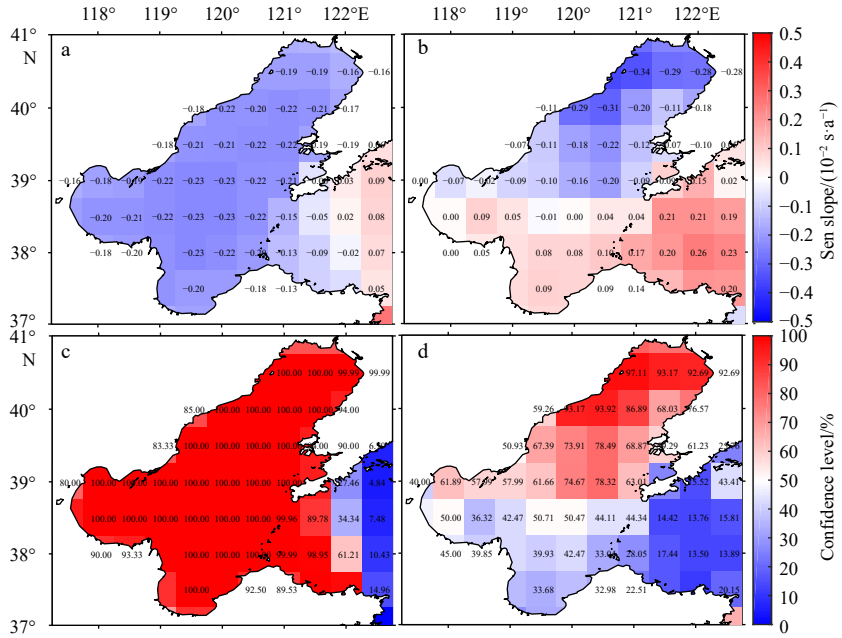

Fig. 15. Heatmaps of inter-annual trend and confidence levels in mean (a, c) and 95th percentile (b, d) C-MWP.

mean trends for MWP are also negative, with Sen slope of –0.17 s/a for combined wave, –0.13 s/a for wind wave and –0.24 s/a for swell.

The various analysis will provide a possible reference for harbor, coastal and offshore engineering in this area.

Acknowledgements

We gratefully thank the respected reviewers for their deep and careful work for this paper.

References

Aboobacker V M, Shanas P R. 2018. The climatology of Shamals in the Arabian Sea-Part 1: surface winds. International Journal of Climatology, 38(12): 4405–4416, doi: 10.1002/joc.5711

Aydoğan B, Ayat B. 2018. Spatial variability of long-term trends of significant wave heights in the Black Sea. Applied Ocean Research, 79: 20–35, doi: 10.1016/j.apor.2018.07.001

Bacon S, Carter D J T. 1991. Wave climate changes in the North Atlantic and North Sea. International Journal of Climatology, 11(5): 545–558

Dee D P, Uppala S M, Simmons A J, et al. 2011. The ERA-interim reanalysis: configuration and performance of the data assimilation system. Quarterly Journal of the Royal Meteorological Society, 137(656): 553–597, doi: 10.1002/qj.828

Ding Yihui, Wang Zunya, Sun Ying. 2008. Inter-decadal variation of the summer precipitation in East China and its association with decreasing Asian summer monsoon. Part I: observed evidences. International Journal of Climatology, 28(9): 1139–1161, doi: 10.1002/joc.1615

Goovaerts P. 2000. Geostatistical approaches for incorporating elevation into the spatial interpolation of rainfall. Journal of Hydrology, 228(1–2): 113–129, doi: 10.1016/S0022-1694(00)00144-X

Guo Weijun, Zhang Shuo, Wu Guoxiang. 2019. Quantitative oil spill risk from offshore fields in the Bohai Sea, China. Science of the Total Environment, 688: 494–504, doi: 10.1016/j.scitotenv.2019.06.226

Haxel J H, Holman R A, 2004. The sediment response of a dissipative beach to variations in wave climate. Marine Geology, 206(1–4): 73–99

Hersbach H, Bell B, Berrisford P, et al. 2020. The ERA5 global reanalysis. Quarterly Journal of the Royal Meteorological Society, 146(730): 1999–2049, doi: 10.1002/qj.3803

Hirsch R M, Slack J R, Smith R A. 1982. Techniques of trend analysis for monthly water quality data. Water Resources Research, 18: 107–121, doi: 10.1029/WR018i001p00107

Kang Shugang, Wang Xulong, Roberts H M, et al. 2018. Late Holocene anti-phase change in the East Asian summer and winter monsoons. Quaternary Science Reviews, 188: 28–36, doi: 10.1016/j.quascirev.2018.03.028

Kundzewicz Z W, Robson A. 2000. Detecting Trend and Other Changes in Hydrological Data. Geneva: World Climate Programme and Monitoring

Liang Bingchen, Liu Xin, Li Huajun, et al. 2016. Wave climate hindcasts for the Bohai Sea, Yellow Sea, and East China Sea. Journal of Coastal Research, 32(1): 172–180

Liu Min, Zhao Dongliang. 2019. Comprehensive studies on wind and wave climates in China Seas based on ERA-20C reanalysis data. Periodical of Ocean University of China, 49(7): 1–10

Lv Xiangcui, Yuan Dekui, Ma Xiaodi, et al. 2014. Wave characteristics analysis in Bohai Sea based on ECMWF wind field. Ocean Engineering, 91: 159–171, doi: 10.1016/j.oceaneng.2014.09.010

Mahmoodi K, Ghassemi H, Razminia A. 2019. Temporal and spatial characteristics of wave energy in the Persian Gulf based on the ERA5 reanalysis dataset. Energy, 187: 115991, doi: 10.1016/j.energy.2019.115991

Mann H B. 1945. Nonparametric tests against trend. Econometrica. 13(3): 245–259

Ren Huiru, Li Guosheng, Cui Linlin, et al. 2017. Simulating wave climate fluctuation in the Bohai Sea related to oscillations in the East Asian circulation over a sixty year period. Journal of Coastal Research, 33(4): 829–838, doi: 10.2112/JCOASTRES-D-15-00209.1

Semedo A, Sušelj K, Rutgersson A, et al. 2011. A global view on the wind sea and swell climate and variability from ERA-40. Journal of Climate, 24(5): 1461–1479, doi: 10.1175/2010JCLI3718.1

Semedo A, Vettor R, Breivik Ø, et al. 2015. The wind sea and swell waves climate in the Nordic seas. Ocean Dynamics, 65(2): 223–240, doi: 10.1007/s10236-014-0788-4

Sen P K. 1968. Estimates of the regression coefficient based on Kendall's tau. Journal of the American Statistical Association, 63(324): 1379–1389, doi: 10.1080/01621459.1968.10480934

Sun Liancheng. 1991. Analysis of wave characteristics of the west offshore area of the Bohai Bay. Journal of Oceanography of Huanghai & Bohai Seas, 9(3): 50–58

Teng Xuechun, Wu Xiujie. 1994. A study on the characteristics of annual extreme and design waves in the south region of the Bohai Sea. Journal of Oceanography of Huanghai & Bohai Seas, 12(3): 3–12

Theil H. 1992. A rank-invariant method of linear and polynomial regression analysis. In: Raj B, Koerts J, eds. Henri Theil's Contributions to Economics and Econometrics. Dordrecht: Springer, 345–381

Tobler W R. 1970. A computer movie simulating urban growth in the Detroit region. Economic Geography, 46(S1): 234–240

Vanem E, Bitner-Gregersen E M. 2012. Stochastic modelling of long-term trends in the wave climate and its potential impact on ship structural loads. Applied Ocean Research, 37: 235–248, doi: 10.1016/j.apor.2012.05.006

Vanem E, Walker S E. 2013. Identifying trends in the ocean wave climate by time series analyses of significant wave height data. Ocean Engineering, 61: 148–160, doi: 10.1016/j.oceaneng.2012.12.042

Wang Daolong, Hua Feng, Jiang Zhihui. 2010. Application of coastal wave model SWAN to Liaodong Bay. Advances in Marine Science, 28(3): 285–291

Wang Zhifeng, Wu Kejian, Zhou Liangming, et al. 2012. Wave characteristics and extreme parameters in the Bohai Sea. China Ocean Engineering, 26(2): 341–350, doi: 10.1007/s13344-012-0026-0

Wu Wenfan, Li Peiliang, Zhai Fangguo, et al. 2020. Evaluation of different wind resources in simulating wave height for the Bohai, Yellow, and East China Seas (BYES) with SWAN model. Continental Shelf Research, 207: 104217, doi: 10.1016/j.csr.2020.104217

Yang Xiaochen, Zhang Qinghe. 2013. Joint probability distribution of winds and waves from wave simulation of 20 years (1989–2008) in Bohai Bay. Water Science and Engineering, 6(3): 296–307

Yin Baoshu, Hou Yijun, Cheng Minghua, et al. 2001. Numerical study of the influence of waves and tide-surge interaction on tide-surges in the Bohai Sea. Chinese Journal of Oceanology and Limnology, 19(2): 97–102, doi: 10.1007/BF02863032

Young I R, Ribal A. 2019. Multiplatform evaluation of global trends in wind speed and wave height. Science, 364(6440): 548–552, doi: 10.1126/science.aav9527

Zheng Chongwei, Pan jing, Li Chongyin. 2016. Global oceanic wind speed trends. Ocean & Coastal Management, 129: 15–24

Zhu Di, Cheng Ximeng, Zhang Fan, et al. 2020. Spatial interpolation using conditional generative adversarial neural networks. International Journal of Geographical Information Science, 34(4): 735–758, doi: 10.1080/13658816.2019.1599122